Large Anomalous Frequency Shift in Perpendicular Standing Spin Wave Modes in BiYIG Films Induced by Thin Metallic Overlayers

Byung Hun Lee⊙, Takian Fakhrul, Caroline A. Ross, and Geoffrey S. D. Beach[*]

Department of Materials Science and Engineering, Massachusetts Institute of Technology, Cambridge, Massachusetts 02139, USA

Interface-driven effects on magnon dynamics are studied in magnetic insulator-metal bilayers using Brillouin light scattering. It is found that the Damon-Eshbach modes exhibit a significant frequency shift due to interfacial anisotropy generated by thin metallic overlayers. In addition, an unexpectedly large shift in the perpendicular standing spin wave mode frequencies is also observed, which cannot be explained by anisotropy-induced mode stiffening or surface pinning. Rather, it is suggested that additional confinement may result from spin pumping at the insulator-metal interface, which results in a locally overdamped interface region. These results uncover previously unidentified interface-driven changes in magnetization dynamics that may be exploited to locally control and modulate magnonic properties in thin-film heterostructures.

Magnetic insulators (MI) such as $Y_3Fe_5O_{12}$ (YIG) have been widely studied for spintronic and magnonic applications due to their low damping and longer magnon diffusion length [1,2]. Although much past work involved bulk crystals or thick films [3], attention has recently turned to nanometer-scale films [4,5]. In such films, substrate strain can be engineered to induce perpendicular magnetic anisotropy (PMA) [6,7], and heavy metal (HM) overlayers can induce interfacial phenomena including spin-orbit torques (SOTs) [8,9] and the Dzyaloshinskii-Moriya interaction (DMI) [10–12]. Recently, epitaxial Bi-substituted YIG (BiYIG) was found to exhibit ultralow damping and strain-induced PMA [13], and to facilitate ultrafast SOT-driven domain wall motion to its relativistic limits [14]. The combination of novel properties, electrically controlled magnetization dynamics, and tunable interfacial interactions make HM/MI bilayer structures attractive for nonvolatile magnetic memories and logic devices [7,8,15–17], as well as magnonic [18,19] and hybrid systems [20–23] that exploit low-dissipation dynamics. Understanding interfacial effects on dynamics in metal-MI structures is crucial to engineering such devices.

It was recently found that metallic layers in contact with thin magnetic garnet films can generate an easy-plane interfacial anisotropy through Rashba spin-orbit coupling (SOC) [24]. Here, we show that this interface-induced anisotropy leads to the expected frequency shift of the magnetostatic (Damon Eshbach, DE) spin wave modes, but those metallic overlayers also generate an anomalous frequency shift of the perpendicular standing wave (PSSW) modes that cannot be accounted for by known mechanisms. The effect remains prominent in BiYIG films with thicknesses up to 70 nm, in contrast to other interfacial phenomena that are usually only important in films with a

thickness of order 1 nm. We posit that the metallic interface generates a localized increase in interfacial damping via spin pumping that substantially damps oscillations proximate to the adjacent metal overlayer, [25] restricting the PSSW mode to an effective thickness that is less than the nominal film thickness and, hence enhancing its frequency. This work identifies new interfacial phenomena that can be used to control spin wave dynamics and gives new insights into the effects of metal-insulator interfaces on magnetization dynamics.

A series of perpendicularly magnetized BiYIG films with thicknesses (t_{BiYIG}) spanning 2.4 to 70 nm was grown using pulsed laser deposition as described elsewhere [14,26]. Films were grown on $Gd_3Sc_2Ga_3O_{12}$ (111) substrates except where noted. Film thicknesses were
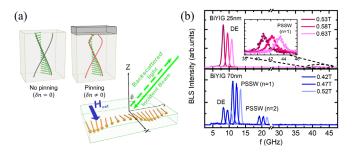

FIG. 1. (a) Schematic of Brillouin light scattering measurement in backscattering geometry. Schematic of $n = 1$ PSSW mode without interfacial pinning in magnetic film and with interfacial pinning with metal overlayer. (b) Exemplary BLS spectra for DE modes and PSSW modes in a 25 and 70 nm thick BiYIG film with several applied fields. PSSW modes up to $n = 2$ are experimentally measured for 70 nm film. A nonmagnetic phonon mode is excluded from the plotted region at the horizontal axis break.

confirmed by using x-ray reflectometry and high-resolution x-ray diffraction. Fully strained epitaxial growth was confirmed by high-resolution x-ray diffraction as well as reciprocal space mapping for the 70 nm film [Fig. S1(a) [27]]. Vibrating sample magnetometry and the polar magneto-optical Kerr effect measurements confirmed that the films exhibited perpendicular magnetic anisotropy with near-bulk saturation magnetization $M_s \approx 140$ kA/m. (See Supplemental Material [27], Sec. S1 for details.) On each film, an array of ~ 1 mm^2 metallic overlayers (Pt, Cu, Au, Ta, and Ti) was deposited using shadow masking and dc magnetron sputtering. Cu, Ta, and Ti layers were capped with 2 nm Pt or Au layers to prevent oxidation.

To quantify the effects on magnetic properties, and to study the influence on magnetization dynamics, we used Brillouin light scattering (BLS) in the Damon-Eshbach (DE) geometry [Fig. 1(a)]. An in-plane external field H_x was applied along the x axis and incident laser illumination (wavelength $\lambda = 532$ nm) was inclined by an angle θ from the surface normal in a plane perpendicular to the field axis. The in-plane component of the magnon wave vector lies along the y axis with the wave vector transfer given by $q_{\parallel} = (4\pi/\lambda)\sin\theta$ [28].

In this geometry, both the DE and the perpendicular standing spin wave modes can be detected, as seen in Fig. 1(b) for $t_{\text{BiYIG}} = 25$ and 70 nm. The respective mode frequencies f_{DE} and f_{PSSW} are given by [29,30]

$$f_{\text{DE}} = \frac{\mu_0\gamma_{\text{eff}}}{2\pi}\sqrt{\left[H_x + \frac{2A}{\mu_0 M_s}q_{\parallel}^2\right]\left[H_x + \frac{2A}{\mu_0 M_s}q_{\parallel}^2 - H_{k,\text{eff}}\right] + \left(\frac{M_s}{2}\right)^2(1 - \exp(-2q_{\parallel}t))} \tag{1}$$

and

$$f_{\text{PSSW}} = \frac{\mu_0\gamma_{\text{eff}}}{2\pi}\sqrt{\left[H_x + \frac{2A}{\mu_0 M_s}(q_{\parallel}^2 + \kappa_n^2)\right]\left[H_x + \frac{2A}{\mu_0 M_s}(q_{\parallel}^2 + \kappa_n^2) - H_{k,\text{eff}}\right]}. \tag{2}$$

Here, μ_0 is the vacuum permeability, γ_{eff} is the effective gyromagnetic ratio that accounts for the coupled dynamics of the individual ferrimagnetic sublattices, [14,17,31] and A is the exchange constant. $H_{k,\text{eff}}$ is the effective perpendicular anisotropy field, given by $H_{k,\text{eff}} = H_u - M_s$, where H_u is the uniaxial out-of-plane anisotropy field defined as $H_u = (2K_u/\mu_0 M_s)$ for a uniaxial anisotropy constant K_u. The term κ_n is the out-of-plane wave vector component, which is quantized for PSSW modes [32,33]. In the absence of surface spin pinning, [34] $\kappa_n = n\pi/t_{\text{BiYIG}}$ with integer n. Finally, DMI shifts the mode frequencies by $\pm(\gamma_{\text{eff}}/\pi M_s)Dq_{\parallel}$, where the $+$ $(-)$ sign corresponds to the Stokes (anti-Stokes) peak [35]. In the Supplemental Material [27], we confirmed that there is no experimentally measurable DMI for BiYIG films with or without Pt, consistent with the conclusions reported in Ref. [10]. We therefore assume that the primary role of metal layers on the DE mode dynamics is through a contribution to the interface anisotropy.

We first focus on the DE modes, for which the exchange contribution is small. To quantify the overlayer-induced anisotropy change, we measured f_{DE} versus H_x at $q_{\parallel} = 0$ [Fig. 2(a)], from which $H_{k,\text{eff}}$ and γ_{eff} can be independently extracted [see Eq. (1)]. For each film thickness, the metal overlayers were deposited in discrete regions of the same sample, so that the metal-induced frequency shifts can be determined unambiguously. This measurement probes the uniform (Kittel) mode, which corresponds to the FMR mode measured in Refs. [24,25]. We measure $\gamma_{\text{eff}}/2\pi \approx 26.2$ GHz/T for all films studied here, independent of t_{BiYIG} and of the presence of metal overlayers. However,
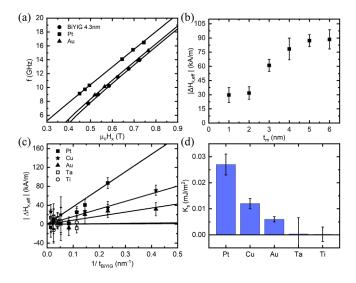

FIG. 2. (a) Frequency of DE modes measured at $q_{\parallel} = 0$ as a function of the applied magnetic field, $\mu_0 H_x$. Solid lines are fits to Eq. (1) in the text. (b) Metal-induced change in effective anisotropy, $\Delta H_{k,\text{eff}}$, as a function of Pt overlayer thickness, on a 4.3 nm BiYIG film. (c) $\Delta H_{k,\text{eff}}$ plotted against inverse BiYIG film thickness, $1/t_{\text{BiYIG}}$, for each metal overlayer. Solid lines are linear fits. (d) Extracted surface anisotropy K_s for each nonmagnetic metal overlayer studied.

metal overlayers change $H_{k,\text{eff}}$ significantly, as seen in Fig. 2(a) for Pt and Au on BiYIG (4.3 nm). The dependence of $\Delta H_{k,\text{eff}} \equiv H_{k,\text{eff}}|_{\text{metal}} - H_{k,\text{eff}}|_{\text{bare}}$ on Pt metal layer thickness (t_m) is plotted in Fig. 2(b). A nominal thickness of just 1 nm is sufficient to change the anisotropy measurably, and the PMA decreases with increasing t_m up to $t_m \approx 4$ nm, at which point $\Delta H_{k,\text{eff}}$ saturates. Since $\Delta H_{k,\text{eff}} < 0$, we infer that the Pt generates an easy-plane anisotropy. The thickness dependence is attributed to an island growth mechanism as is typical for noble metal growth on an oxide, which would lead to incomplete film coverage at low t_m.

Similar measurements were performed for a wide range of t_{BiYIG}, for several metallic overlayer species, all with $t_m = 4$ nm to ensure saturation of the metal-induced anisotropy change. The extracted $\Delta H_{k,\text{eff}}$ are plotted versus $1/t_{\text{BiYIG}}$ in Fig. 2(c), where the linear correlation implies a surface-driven anisotropy change, $\Delta H_{k,\text{eff}} = (2K_s/\mu_0 M_s) \times (1/t_{\text{BiYIG}})$, with K_s the surface (interface) anisotropy energy density. The extracted K_s for each metal are plotted in Fig. 2(d). We find that $|K_s(\text{Pt})| > |K_s(\text{Cu})| > |K_s(\text{Au})|$, whereas for Ta and Ti, K_s is smaller than the experimental uncertainty. We note that the BLS signal for Ta and Ti-covered films is significantly reduced for low t_{BiYIG} to an extent that precludes measurements on film thicknesses that are omitted in Fig. 2(c). The value of K_s for Pt/BiYIG is ~2 orders of magnitude smaller than in metallic systems such as Pt/Co, and its sign is different, pointing to a qualitatively different mechanistic origin. Compared to the results reported in Ref. [24] using TmIG, the K_s value that we find for Pt/BiYIG is about half as large as reported for Pt/TmIG, and moreover, the ordering of metals by their $|K_s|$ was reported to be Ti > Ta > Au > Cu > Pt, which is opposite to what we find here. The reason for the difference is not understood, but it may point to the influence of the rare earth element in the garnet studied in Ref. [24], which is not present in BiYIG. We note that differences in surface anisotropy between the top and bottom surface has also been shown to give rise to nonreciprocity of DE mode [36], but the effect is too small in the present samples to be experimentally resolved. (See Sec. S5 of the Supplemental Material [27] for details.)

We now turn to the PSSW modes, which are distinguished from the DE modes by a strong thickness dependence of the mode frequencies due to the exchange term in Eq. (2) that arises due to standing waves confined along the film thickness. PSSW modes are visible in the BLS spectra for $t_{\text{BiYIG}} = 25$, 40, and 70 nm, the latter of which exhibits two experimentally accessible modes [see Fig. 1(b)]. For thinner films, the PSSW frequencies occur outside of the instrumental range of our BLS system. We confirmed the mode assignments by fitting the mode frequencies to Eqs. (1) and (2), as shown in Fig. S3(a). The PSSW mode frequencies for all three thicknesses can be well fitted with a single exchange constant $A = 4.0 \pm 0.3$ pJ/m (see Sec. S3 of the Supplemental Material [27]), which agrees well with the accepted bulk value [37].
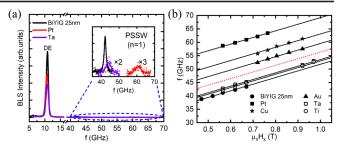

FIG. 3.   (a) Exemplary BLS spectra of bare 25 nm BiYIG and BiYIG covered with Pt and Ta. Inset is enlarged PSSW modes, magnified 2 and 3 times its intensity for Pt and Ta overlayers, respectively. (b) The frequency of measured PSSW modes as a function of $\mu_0 H_x$ with $q_\parallel = 0$. The expected frequency with measured A and K_s with Pt overlayer is plotted with a dotted red line.

Similar to the DE modes, we find a significant frequency shift for the PSSW modes upon the addition of metallic overlayers, as seen in Fig. 3(a). Frequency shifts are evident even for the thickest films ($t_{\text{BiYIG}} = 70$ nm) and for metal layers (Ta and Ti) whose influence on the DE modes was not resolvable. Although the K_s contribution to $H_{k,\text{eff}}$ should increase the mode frequency, we find that the magnitude of the observed frequency shift is much larger than what can be accounted for by the metal-induced change in $H_{k,\text{eff}}$ in Eq. (2). Figure 3(b) shows the measured PSSW mode frequency versus H_x for $t_{\text{BiYIG}} = 25$ nm with several metal overlayers, as well as the computed f versus H_x using Eq. (2) with the measured A and K_s for Pt. We see that $\Delta H_{k,\text{eff}}$ should yield only a very small PSSW frequency shift in the case of Pt, contrary to our observations.

Since the PSSW modes are standing modes confined along the film thickness, one could anticipate that surface-driven phenomena may play a significant role in modifying the PSSW behavior. Surface anisotropy can not only change $H_{k,\text{eff}}$ but also influences the PSSW boundary conditions through a phenomenon termed surface spin pinning [Fig. 1(a)]. In this case, the transverse wave number satisfies [34,38]

$$\tan(\kappa_n t) = \frac{\kappa_n(\xi_0 + \xi_t)}{\kappa_n^2 - \xi_0 \xi_t}, \qquad (3)$$

where ξ_0 and ξ_t are pinning parameters at the bottom and top interface, respectively. When $\xi_0 = \xi_t = 0$, Eq. (3) reduces to $\tan(\kappa_n t) = 0$, which yields $\kappa_n = n\pi/t$, where $n = 1, 2, 3, \ldots$ [39]. However, for finite surface spin pinning, solutions to Eq. (3) take the form $\kappa_n = (n + \delta n)\pi/t$ with nonzero δn, which leads to an enhancement of the exchange contribution to the mode frequency. In the Supplemental Material [27], we show that the thickness-dependent spectra in the uncovered BiYIG films are consistent with a value $\delta n \approx 0$, indicating that surface spin pinning is small or absent for the bare films. We therefore
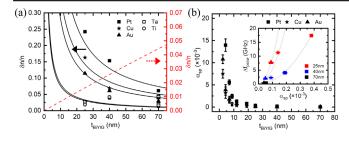
FIG. 4. (a) The extracted $\delta n/n$ for different metal overlayers is plotted versus t_{BiYIG}. Solid lines are fits to $\delta n/n = \Delta t/t$. The dotted red line is a plot of computed $\delta n/n$ for Pt with measured A and K_s. (b) The α_{sp} given by the difference of α_{eff} with and without metal overlayers of Pt, Cu, and Au, is plotted as a function of t_{BiYIG}. The inset shows the Δf_{PSSW} for $n = 1$ mode with Pt, Cu, and Au overlayer plotted as a function of the α_{sp} for BiYIG film thicknesses 25, 40, and 70 nm. Lines in the inset are visual guides.

take $\xi_0 = 0$ in Eq. (3) and assume ξ_t is nonzero when the metal-induced K_s are present. With this assumption, $\tan(\kappa_n t) = (\xi_t/\kappa_n)$, where ξ_t is related to K_s in the surface spin pinning model by $\xi_t = -A/K_s$ when the magnetization is oriented perpendicular to the film normal as is the case for the range of H_x used here [39,40].

In Fig. 4(a) we plot the expected δn computed using the measured A and K_s for Pt. We compare the computed value to δn extracted by fitting the PSSW peak frequencies to Eq. (2) with A and K_s fixed and with $\kappa_n = (n + \delta n)\pi/t$ being the sole fitting parameter. The results show two striking features. First, the surface spin pinning model predicts that δn increases with increasing film thickness t_{BiYIG}, whereas we find that δn varies approximately as $1/t_{BiYIG}$ experimentally. Second, the magnitude of δn predicted by the spin pinning theory is an order of magnitude smaller than the measured quantities. We therefore conclude that surface spin pinning cannot account for the large PSSW frequency shifts observed experimentally.

We can explain the data phenomenologically by instead writing $\kappa_n = n\pi/(t - \Delta t)$, which is equivalent to $\kappa_n = (n + \delta n)\pi/t$ with $\delta n/n = \Delta t/t$ in the limit $\Delta t \ll t$. This corresponds physically to an interfacial region in which the standing wave is excluded, reducing the effective confining distance by Δt. The solid lines in Fig. 4(a) show fits to this phenomenological expression, which yield $\Delta t = 5.2 \pm 0.4$, 3.6 ± 0.5, 2.8 ± 0.1, 0.8 ± 0.2, and 1.0 ± 0.4 nm for Pt, Cu, Au, Ta, and Ti, respectively. This expression is consistent with the observed PSSW frequency shift. We note that metal deposition results in the formation of at most $\sim$0.6 nm of a magnetically dead layer at the interface, and so this effect alone cannot explain our observations. (see Sec. S1 of the Supplemental Material [27] for details).

To motivate a possible physical origin for such behavior, we consider interfacial spin pumping associated with the dynamics. The angular momentum transfer creates a torque that is mathematically equivalent to Gilbert damping torque,

with a magnitude $\alpha_{sp} = (\hbar\gamma_{eff}/M_s t_{BiYIG})\text{Re}\{g_{\uparrow\downarrow}\}$, where $g_{\uparrow\downarrow}$ is the interfacial spin mixing conductance. We extracted the effective damping α_{eff} from the slope of the DE mode BLS linewidth versus field [41–43] (see Supplemental Material [27] Sec. S4), and determined α_{sp} as the difference of α_{eff} with and without a metal overlayer. In Fig. 4(b), we plot α_{sp} versus t_{BiYIG} for BiYIG capped with Pt, Cu, and Au, as well as fits that confirm the $1/t_{BiYIG}$ dependence. We extract values for $g_{\uparrow\downarrow}$ of 4.6 ± 1.2 2.1 ± 0.5, 3.5 ± 1.0 nm^{-2} for Pt, Cu, and Au, respectively, similar to values reported elsewhere [25,44,45]. We see that the trend of $g_{\uparrow\downarrow}$ with varying metal overlayer follows that of Δt, suggesting that increased spin pumping tends to increase the quenched thickness of the dynamically quenched region. This correlation is also seen in the inset of Fig. 4(b), where the metal-induced frequency shift is plotted versus α_{sp} for varying t_{BiYIG} and varying metal overlayer. For a given metal layer, we see an approximately quadratic increase in Δf_{PSSW} with α_{sp}, since α_{sp} scales as $1/t_{BiYIG}$ and Δf_{PSSW} scales approximately as $(1/t_{BiYIG})^2$ [since the exchange term dominates in Eq. (2)]. For a given film thickness Δf_{PSSW} increases with increasing α_{sp}, corresponding to metals with larger $g_{\uparrow\downarrow}$. This observation suggests that interfacial spin pumping plays an important role in the observed PSSW frequency shifts.

Magnetization dynamics in thin films is usually described by assuming a uniform effective damping α_{eff} that includes intrinsic (α_0) and spin-pumping contributions. However, the torque responsible for α_{sp} is localized at the insulator-metal interface where the SOC plays an essential role, and the local effective damping should be much larger in this region [46]. For dynamics that are uniform through the film thickness, such as uniform precession or domain wall motion, it is reasonable to describe the dynamics using a single, effective dissipation factor accounting for the total dissipation through the film thickness. However, PSSW modes are by definition nonuniform through the film thickness and should therefore be sensitive to spatial variations in the dissipation. In the present case, $\alpha_{sp} \approx 0.014$ for Pt/BiYIG (4.3 nm), implying that the effective damping torque is very strong in the interfacial region. By contrast, for $t_{BiYIG} = 70$ nm without Pt, we find a damping $\alpha_0 \approx 8 \times 10^{-4}$. For a thick BiYIG, one would therefore expect the damping far from the interface to be $\sim$20 times smaller than near the metal interface. We suggest that this interface-enhanced damping quenches the PSSW dynamics in a thin interfacial region, giving rise to the phenomenological decrease Δt in the effective confining thickness. In contrast, the quenching negligibly affects the resonance frequency of DE modes, since those modes propagate along the film surface and are relatively thickness independent within the regime studied here. When the boundary condition is modified by the local spin pumping effect, the averaged frequency of the uniform mode ($q_{\parallel} = 0$) is

unchanged from the case with unpinned spins [Eq. (1)], while a frequency nonreciprocity is introduced for the propagating DE modes, as studied in systems with asymmetric surface anisotropy [36] or DMI [47].

In conclusion, we have studied the effects of metallic overlayers on the DE and PSSW modes in BiYIG films with low intrinsic damping. We find frequency shifts of the DE modes that can be well understood by a surface anisotropy contribution at the metal-insulator interface, which reduces the net PMA and hence alters the mode frequency. We also find metal-induced frequency shifts in the PSSW modes but conclude that the metal-induced surface anisotropy cannot account for its magnitude either through the change in $H_{k,\mathrm{eff}}$ or the effects of K_s on the surface boundary conditions. We propose a phenomenological model that can describe the observed shifts in terms of an interfacial region that is excluded from the through-thickness PSSW excitation, confining the PSSW modes within an effective thickness that is smaller than the characterized film thickness. In the presence of the SOC at the HM/MI interface, the transfer of spin momentum and polarization and the resulting spin pumping are governed by the strength of the SOC. We suggest that the spin-pumping torque that plays a role akin to damping quenches the through-thickness magnetic excitation near the interface where the effective damping is large, which would qualitatively explain the anomalously-large metal-induced frequency shifts. Therefore, in the study of spin-pumping associated with the PSSW mode, one should always consider adopting the effective thickness model developed in this work. Although the exact mechanism remains to be understood, our work identifies for the first time a significant new interface-driven impact on magnetization dynamics which could be exploited to locally control the magnon mode resonances in spintronic devices such as magnonic crystals.

---

*To whom all correspondence to should be addressed.
gbeach@mit.edu

[1] A. A. Serga, A. V. Chumak, and B. Hillebrands, YIG magnonics, J. Phys. D **43**, 264002 (2010).

[2] H. Wang, J. Chen, T. Liu, J. Zhang, K. Baumgaertl, C. Guo, Y. Li, C. Liu, P. Che, S. Tu, S. Liu, P. Gao, X. Han, D. Yu, M. Wu, D. Grundler, and H. Yu, Chiral Spin-Wave Velocities Induced by All-Garnet Interfacial Dzyaloshinskii-Moriya Interaction in Ultrathin Yttrium Iron Garnet Films, Phys. Rev. Lett. **124**, 027203 (2020).

[3] S. Klingler, A. Chumak, T. Mewes, B. Khodadadi, C. Mewes, C. Dubs, O. Surzhenko, B. Hillebrands, and A. Conca, Measurements of the exchange stiffness of YIG films using broadband ferromagnetic resonance techniques, J. Phys. D **48**, 015001 (2015).

[4] H. Chang, P. Li, W. Zhang, T. Liu, A. Hoffmann, L. Deng, and M. Wu, Nanometer-thick yttrium iron garnet films with extremely low damping, IEEE Magn. Lett. **5**, 6700104 (2014).

[5] H. Yu, O. D'Allivy Kelly, V. Cros, R. Bernard, P. Bortolotti, A. Anane, F. Brandl, R. Huber, I. Stasinopoulos, and D. Grundler, Magnetic thin-film insulator with ultra-low spin wave damping for coherent nanomagnonics, Sci. Rep. **4**, 6848 (2014).

[6] E. R. Rosenberg, L. Beran, C. O. Avci, C. Zeledon, B. Song, C. Gonzalez-Fuentes, J. Mendil, P. Gambardella, M. Veis, C. Garcia, G. S. D. Beach, and C. A. Ross, Magnetism and spin transport in rare-earth-rich epitaxial terbium and europium iron garnet films, Phys. Rev. Mater. **2**, 094405 (2018).

[7] A. Quindeau *et al.*, $Tm_3Fe_5O_{12}/Pt$ heterostructures with perpendicular magnetic anisotropy for spintronic applications, Adv. Electron. Mater. **3**, 1600376 (2017).

[8] C. O. Avci, A. Quindeau, C. F. Pai, M. Mann, L. Caretta, A. S. Tang, M. C. Onbasli, C. A. Ross, and G. S. D. Beach, Current-induced switching in a magnetic insulator, Nat. Mater. **16**, 309 (2017).

[9] C. O. Avci, A. Quindeau, M. Mann, C. F. Pai, C. A. Ross, and G. S. D. Beach, Spin transport in as-grown and annealed thulium iron garnet/platinum bilayers with perpendicular magnetic anisotropy, Phys. Rev. B **95**, 115428 (2017).

[10] L. Caretta *et al.*, Interfacial Dzyaloshinskii-Moriya interaction arising from rare-earth orbital magnetism in insulating magnetic oxides, Nat. Commun. **11**, 1090 (2020).

[11] A. J. Lee, A. S. Ahmed, J. Flores, S. Guo, B. Wang, N. Bagués, D. W. Mccomb, and F. Yang, Probing the Source of the Interfacial Dzyaloshinskii-Moriya Interaction Responsible for the Topological Hall Effect in Metal/$Tm_3Fe_5O_{12}$ Systems, Phys. Rev. Lett. **124**, 107201 (2020).

[12] S. Ding *et al.*, Interfacial Dzyaloshinskii-Moriya interaction and chiral magnetic textures in a ferrimagnetic insulator, Phys. Rev. B **100**, 100406 (2019).

[13] L. Soumah, N. Beaulieu, L. Qassym, C. Carrétéro, E. Jacquet, R. Lebourgeois, J. Ben Youssef, P. Bortolotti, V. Cros, and A. Anane, Ultra-low damping insulating magnetic thin films get perpendicular, Nat. Commun. **9**, 3355 (2018).

[14] L. Caretta, S. H. Oh, T. Fakhrul, D. K. Lee, B. H. Lee, S. K. Kim, C. A. Ross, K. J. Lee, and G. S. D. Beach, Relativistic kinematics of a magnetic soliton, Science **370**, 1438 (2020).

[15] B. Dieny *et al.*, Opportunities and challenges for spintronics in the microelectronics industry, Nat. Electron. **3**, 446 (2020).

[16] C. O. Avci, E. Rosenberg, L. Caretta, F. Büttner, M. Mann, C. Marcus, D. Bono, C. A. Ross, and G. S. D. Beach, Interface-driven chiral magnetism and current-driven domain walls in insulating magnetic garnets, Nat. Nanotechnol. **14**, 561 (2019).

[17] L. Caretta *et al.*, Fast current-driven domain walls and small skyrmions in a compensated ferrimagnet, Nat. Nanotechnol. **13**, 1154 (2018).

[18] A. V. Chumak, A. A. Serga, and B. Hillebrands, Magnonic crystals for data processing, J. Phys. D **50**, 244001 (2017).

[19] A. V. Chumak, T. Neumann, A. A. Serga, B. Hillebrands, and M. P. Kostylev, A current-controlled, dynamic magnonic crystal, J. Phys. D **42**, 205005 (2009).

[20] H. Qin, S. J. Hämäläinen, and S. Van Dijken, Exchange-torque-induced excitation of perpendicular standing spin waves in nanometer-thick YIG films, Sci. Rep. **8**, 5755 (2018).

[21] Y. Li et al., Coherent Spin Pumping in a Strongly Coupled Magnon-Magnon Hybrid System, Phys. Rev. Lett. **124**, 117202 (2020).

[22] S. Klingler et al., Spin-Torque Excitation of Perpendicular Standing Spin Waves in Coupled YIG/Co Heterostructures, Phys. Rev. Lett. **120**, 127201 (2018).

[23] J. Chen, C. Liu, T. Liu, Y. Xiao, K. Xia, G. E. W. Bauer, M. Wu, and H. Yu, Strong Interlayer Magnon-Magnon Coupling in Magnetic Metal-Insulator Hybrid Nanostructures, Phys. Rev. Lett. **120**, 217202 (2018).

[24] A. J. Lee, A. S. Ahmed, B. A. McCullian, S. Guo, M. Zhu, S. Yu, P. M. Woodward, J. Hwang, P. C. Hammel, and F. Yang, Interfacial Rashba-Effect-Induced Anisotropy in Nonmagnetic-Material-Ferrimagnetic-Insulator Bilayers, Phys. Rev. Lett. **124**, 257202 (2020).

[25] Y. Sun et al., Damping in Yttrium Iron Garnet Nanoscale Films Capped by Platinum, Phys. Rev. Lett. **111**, 106601 (2013).

[26] T. Fakhrul, S. Tazlaru, L. Beran, Y. Zhang, M. Veis, and C. A. Ross, Magneto-optical Bi:YIG films with high figure of merit for nonreciprocal photonics, Adv. Opt. Mater. **7**, 1900056 (2019).

[27] See Supplemental Material at http://link.aps.org/supplemental/10.1103/PhysRevLett.130.126703 for sample preparation, characterizations for magnetic properties overlayers measured by VSM and MOKE, determination of DMI and exchange constant in the BiYIG films, assessment of interfacial spin pinning in the bare films, effective damping measured by BLS linewidth measurements, and effect of surface anisotropy on DE modes in thick films, which includes Ref. [6,10,24,25,32,34,36].

[28] T. Sebastian, K. Schultheiss, B. Obry, B. Hillebrands, and H. Schultheiss, Micro-focused Brillouin light scattering: Imaging spin waves at the nanoscale, Front. Phys. **3**, 1 (2015).

[29] S. O. Demokritov, B. Hillebrands, and A. N. Slavin, Brillouin light scattering studies of confined spin waves: Linear and nonlinear confinement, Phys. Rep. **348**, 441 (2001).

[30] B. A. Kalinikos and A. N. Slavin, Theory of dipole-exchange spin wave spectrum for ferromagnetic films with mixed exchange boundary conditions, J. Phys. C **19**, 7013 (1986).

[31] C. D. Stanciu, A. V. Kimel, F. Hansteen, A. Tsukamoto, A. Itoh, A. Kirilyuk, and T. Rasing, Ultrafast spin dynamics across compensation points in ferrimagnetic GdFeCo: The role of angular momentum compensation, Phys. Rev. B **73**, 220402 (2006).

[32] B. A. Kalinikos, M. P. Kostylev, N. v. Kozhus, and A. N. Slavin, The dipole-exchange spin wave spectrum for anisotropic ferromagnetic films with mixed exchange boundary conditions, J. Phys. Condens. Matter **2**, 9861 (1990).

[33] G. Dieterle et al., Coherent Excitation of Heterosymmetric Spin Waves with Ultrashort Wavelengths, Phys. Rev. Lett. **122**, 117202 (2019).

[34] R. F. Soohoo, General exchange boundary condition and surface anisotropy energy of a ferromagnet, Phys. Rev. **131**, 594 (1963).

[35] K. Di, V. L. Zhang, H. S. Lim, S. C. Ng, M. H. Kuok, X. Qiu, and H. Yang, Asymmetric spin-wave dispersion due to Dzyaloshinskii-Moriya interaction in an ultrathin Pt/CoFeB film, Appl. Phys. Lett. **106**, 052403 (2015).

[36] O. Gladii, M. Haidar, Y. Henry, M. Kostylev, and M. Bailleul, Frequency nonreciprocity of surface spin wave in permalloy thin films, Phys. Rev. B **93**, 054430 (2016).

[37] A. P. Malozemoff and J. C. Slonczewski, Magnetic Domain Walls in Bubble Materials (Academic Press, New York, 1979), Chap. 2, p. 15.

[38] G. T. Rado and J. R. Weertman, Spin-wave resonance in a ferromagnetic metal, J. Phys. Chem. Solids **11**, 315 (1959).

[39] A. Gurevich and G. Melkov, Magnetic Oscillations and Waves (CRC Press, London, 1996), Chap. 7, p. 189.

[40] E. Burgos, E. Sallica Leva, J. Gómez, F. Martínez Tabares, M. Vásquez Mansilla, and A. Butera, Surface pinning in ferromagnetic films with perpendicular anisotropy, Phys. Rev. B **83**, 174417 (2011).

[41] K. Di, V. L. Zhang, H. S. Lim, S. C. Ng, M. H. Kuok, J. Yu, J. Yoon, X. Qiu, and H. Yang, Direct Observation of the Dzyaloshinskii-Moriya Interaction in a Pt/Co/Ni Film, Phys. Rev. Lett. **114**, 047201 (2015).

[42] X. Ma, G. Yu, C. Tang, X. Li, C. He, J. Shi, K. L. Wang, and X. Li, Interfacial Dzyaloshinskii-Moriya Interaction: Effect of 5d Band Filling and Correlation with Spin Mixing Conductance, Phys. Rev. Lett. **120**, 157204 (2018).

[43] N. H. Kim, J. Jung, J. Cho, D. S. Han, Y. Yin, J. S. Kim, H. J. M. Swagten, and C. Y. You, Interfacial Dzyaloshinskii-Moriya interaction, surface anisotropy energy, and spin pumping at spin orbit coupled Ir/Co interface, Appl. Phys. Lett. **108**, 142406 (2016).

[44] C. Burrowes, B. Heinrich, B. Kardasz, E. A. Montoya, E. Girt, Y. Sun, Y. Y. Song, and M. Wu, Enhanced spin pumping at yttrium iron garnet/Au interfaces, Appl. Phys. Lett. **100**, 092403 (2012).

[45] B. Heinrich, C. Burrowes, E. Montoya, B. Kardasz, E. Girt, Y. Y. Song, Y. Sun, and M. Wu, Spin Pumping at the Magnetic Insulator (YIG)/Normal Metal (Au) Interfaces, Phys. Rev. Lett. **107**, 066604 (2011).

[46] K. Chen and S. Zhang, Spin Pumping in the Presence of Spin-Orbit Coupling, Phys. Rev. Lett. **114**, 126602 (2015).

[47] M. Kostylev, Interface boundary conditions for dynamic magnetization and spin wave dynamics in a ferromagnetic layer with the interface Dzyaloshinskii-Moriya interaction, J. Appl. Phys. **115**, 233902 (2014).